Analytic Band-to-Trap Tunneling Model Including Electric Field and Band Offset Enhancement

Xujiao Gao
electrical models and simulation
sandia national laboratories
Albuquerque, USA
xngao@sandia.gov

Bert Kerr
mathematics department
new mexico institute of mining and technology
Socorro, USA
gilbert.kerr@nmt.edu

Andy Huang
electrical models and simulation
sandia national laboratories
Albuquerque, USA
ahuang@sandia.gov

Gary Hennigan
electrical models and simulation
sandia national laboratories
Albuquerque, USA
glhenni@sandia.gov

Lawrence Musson
electrical models and simulation
sandia national laboratories
Albuquerque, USA
lcmusso@sandia.gov

Mihai Negoita
electrical models and simulation
sandia national laboratories
Albuquerque, USA
mnegoit@sandia.gov

***Abstract*—We present an analytic band-to-trap tunneling model developed using the open boundary scattering approach. The new model explicitly includes the effect of heterojunction band offset, in addition to the well known electric field effect. Its analytic form enables straightforward implementation into TCAD device and circuit simulators. The model is capable of simulating both electric field and band offset enhanced carrier recombination due to the band-to-trap tunneling in the depletion region near a heterojunction. Simulation results of an InGaP/GaAs heterojunction bipolar transistor reveal that the proposed model predicts significantly increased base currents, because the hole-to-trap tunneling from the base to the emitter is greatly enhanced by the emitter base heterojunction band offset. The results compare favorably with experimental observations. The developed method can be applied to all one dimensional potentials which can be approximated to a good degree such that the approximated potentials lead to piecewise analytic wave functions with open boundary conditions.**

***Index Terms*—band-to-trap tunneling, density of states, band offset, field enhancement factor, heterojunction bipolar transistor**

I. Introduction

Unintentional traps created during fabrication and/or by exposure to radiation environments can significantly alter the electrical properties of semiconductor devices. At a sufficiently high trap density, the band-to-trap tunneling [1] can cause a significant increase in terminal currents, especially under high electric fields [2] [3]. Standard band-to-trap tunneling models, such as those by Schenk [1] [4] and Hurkx [5], are widely incorporated in TCAD (Technology Computer Aided Design) device simulation tools [6] to account for this effect. However, these models were developed for silicon and are, therefore, often unsuitable for modeling heterojunction devices. This is because they do not account for the effect of band offset, which can be significant in heterojunction devices. In fact, as shown recently by Myers et al. [7], the band offset at the emitter-base (E-B) junction in a lattice matched $In_{0.5}Ga_{0.5}P$/GaAs $NP^{+}N$ heterojunction bipolar transistor (HBT) greatly enhances the tunneling of holes from the base to the traps in the emitter. This tunneling substantially increases carrier recombination in the E-B depletion region, leading to large base currents under neutron radiation environments, and consequently exacerbates the degradation of gain due to radiation damage.

In this work, we propose an analytic band-to-trap tunneling model based on Schenk's approach, which includes the effects of both electric field and band offset. We will demonstrate that the model predicts significantly increased base currents in a HBT, due to the strong hole-to-trap tunneling caused not only by the electric field effect, but more importantly by the band offset enhancement. Notably, the analytic form of the model enables straightforward implementation into TCAD device and circuit simulators.

II. Proposed Tunneling Model

Within Schenk's approach [4], the band-to-trap tunneling is modeled as Shockley-Read-Hall (SRH) recombination with field-dependent carrier lifetime, τ, given by

$$\tau(T,F) = \frac{\tau(T,F=0)}{1+g(T,F)}, \tag{1}$$

$$g(T,F) = \frac{\int_0^{E_t} \rho_F(E) \exp\left(\frac{-E}{2k_BT}\right) I_{E/\hbar\omega_0}(z)dE}{\int_{E_t}^{+\infty} \rho_{F=0}(E) \exp\left(\frac{-E}{2k_BT}\right) I_{E/\hbar\omega_0}(z)dE}. \tag{2}$$

Here T and F denote temperature and electric field, respectively; $g(T,F)$ is the field enhancement factor depending on temperature and electric field; E_t is the trap binding energy measured from the corresponding band edge (e.g., conduction band edge for electrons and valence band edge for holes); k_B is the Boltzmann constant; $\rho_{F=0}(E)$ is the zero field energy dependent band density of states (DOS); $\rho_F(E)$ is the three dimensional (3D) tunneling DOS; $I_{E/\hbar\omega_0}(z)$ denotes the modified Bessel function of the first kind with $\hbar\omega_0$ being the optical phonon energy. The argument of the modified Bessel

function is defined as $z = 2S\sqrt{f_B(f_B+1)}$, with S being the Huang-Rhys factor and f_B being the Bose function, i.e., $f_B = [\exp(\hbar\omega_0/k_BT) - 1]^{-1}$.

Characteristics of the band profile, including electric field and band offset, affect the field enhancement factor, $g(T, F)$, through the 3D tunneling DOS, $\rho_F(E)$. Schenk used the constant field DOS expression in his original model [1]. It is a reasonable approximation for homojunction devices, but is inadequate for heterojunction devices. This can be seen from the typical band profile of an $In_{0.5}Ga_{0.5}P/GaAs$ NP^+N HBT in Fig. 1, where the tunneling of holes in the base to traps in the emitter is determined by the valence band profile. It is evident that the valence band deviates significantly from Schenk's constant field assumption.

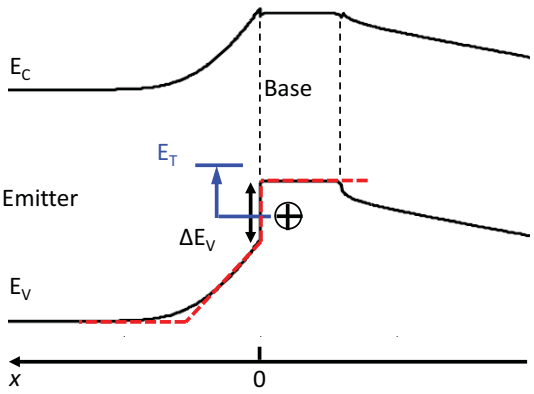

Fig. 1. Typical band profile in the emitter and base regions of an $In_{0.5}Ga_{0.5}P/GaAs$ NP^+N HBT. Here E_C is the conduction band, E_V is the valence band, ΔE_V is the valence band offset, and E_T indicates the trap location. The circle with a plus represents a hole, and the blue arrow denotes the hole-to-trap tunneling path. The red dashed curve is a linearized potential to approximate the actual valence band.

To compute the 3D tunneling DOS for the valence band in Fig. 1, we first assume the potential of interest is in the x direction only, while the y-z plane has a zero potential and carriers are free to move with an effective mass. Then the standard approach [8] is to numerically solve the 1D Schrodinger equation with closed boundary conditions (BCs). This approach results in *discrete* eigen-energies and eigen-functions, which are then used to compute the DOS. However, this method is expensive and difficult to implement into a Message Passing Interface (MPI) based parallel TCAD code. Another option for computing the DOS [9] [10] is utilizing the retarded Green's function, which is often used for open boundary quantum transport modeling and simulation. Determining Green's functions for semiconductor transport problems is, however, notoriously difficult. And it is often more difficult to obtain analytic Green's functions than analytic wave functions for a given potential profile.

To overcome these limitations, we have developed an efficient analytic DOS model based on the open boundary scattering method [11]. In this approach, we first approximate the actual band profile (e.g., the valence band in Fig. 1) using a linearized potential (e.g., the red dashed curve in Fig. 1). Second, we treat the linearized potential as an *open boundary scattering* problem with a *continuous* energy spectrum, which allows us to obtain piecewise analytic wave functions (WFs). Third, we normalize the WFs according to the Dirac delta normalization condition [12]

$$\int_{-\infty}^{+\infty} \psi^*_{E_x}(x)\psi_{E'_x}(x)dx = \delta(E_x - E'_x). \tag{3}$$

For this particular normalization, we discovered that there exists a universal normalization factor. The universal normalization factor is applicable to *any 1D potentials that have open BCs and lead to piecewise analytic wave functions* [13]. It has a very simple form, given by

$$|N|^2 = \frac{m^*}{2\pi\hbar^2 k} \quad \text{with} \quad k = \sqrt{\frac{2m^*E}{\hbar^2}}. \tag{4}$$

Here $|N|^2$ is the normalization factor squared and m^* is the carrier effective mass. Finally, we apply the delta normalized wave functions to compute the 3D DOS using

$$\rho_F(x, E) = \frac{m^*}{\pi\hbar^2}\int_0^{+\infty} |\psi_{E_x}(x)|^2\theta(E - E_x)dE_x, \tag{5}$$

where $\theta(\cdot)$ is the Heaviside step function.

Following the above procedure, we can obtain the 3D tunneling DOS for the linearized potential in Fig. 1 as

$$\rho_F(x, E) = \frac{1}{2\pi^2}\left(\frac{2m^*}{\hbar^2}\right)^{\frac{3}{2}}\int_0^{E^*} \frac{|A_i(\alpha x + \beta)|^2}{|A_i(\beta)|^2 + \frac{\hbar\theta}{E_x}|A'_i(\beta)|^2}\frac{dE_x}{\sqrt{E_x}}. \tag{6}$$

Here $E^* = qFx + V_0 - E_t + E$ with q being the elemental charge, x is the positive distance from the heterojunction, V_0 is the HJ band offset (e.g., ΔE_V in Fig. 1), and $0 \le E \le E_t$. $A_i(\cdot)$ is the Airy function, and $A'_i(\cdot)$ is the first derivative of the Airy function. α, β, and $\hbar\theta$, are given by

$$\alpha = \left(\frac{2m^*qF}{\hbar^2}\right)^{\frac{1}{3}}, \beta = \frac{V_0 - E_x}{\hbar\theta}, \hbar\theta = \left(\frac{\hbar^2q^2F^2}{2m^*}\right)^{\frac{1}{3}}. \tag{7}$$

It is seen that the 3D DOS in (6) involves an integration over the energy, but does not involve any integration over the space. This makes the DOS model amenable to implement in a MPI parallel programming environment, and hence it can be readily implemented into TCAD device and circuit simulators. To efficiently compute the integral in (6), we used the Gauss-Jacobi quadrature scheme [14]. Ten to twenty collocation points (depending on the selected parameter set) were sufficient to ensure an error of less than 1%. We also found that the adaptive quadrature rule [15] works very well for computing the field enhancement factor in (2), since the integrands in both the numerator and the denominator are sharply localized along the energy axis. Lastly, when implementing the DOS and the field enhancement factor in a TCAD simulator, the local electric field is used instead of actually linearizing a potential. Note the local electric field is also widely used for the Schenk model [4] implemented in commercial TCAD simulators [6].

The proposed and Schenk band-to-trap tunneling models were implemented into *Charon*, a multi-dimensional MPI parallel TCAD code developed at Sandia National Laboratories. *Charon* supports the generalized Scharfetter-Gummel discretization [16] and several stabilized finite element discretization schemes [17] [18]. It can be used to simulate arbitrary 2D/3D devices, supports multi-physics capability (i.e., allowing for solving different equations in different regions), and is capable of running large simulations on thousands of processors simultaneously. It has been used to simulate a wide variety of devices, such as HBTs [11], field effect transistors, wide band gap devices (e.g., GaN devices), and transition metal oxide memristors [19] [20].

III. Simulation Results and Discussion

Fig. 2 compares the 3D tunneling DOS for a linearized potential at three locations computed using three different approaches. The parameters used are $m^* = 0.082$, $\hbar\omega_0 = 0.02$ eV, $S = 12.2$, and $E_t = 0.93$ eV, which are close to the values for mid-band gap traps in the $In_{0.5}Ga_{0.5}P$ material. The constant field DOS (black) depends only on the field strength, not on the spatial location, as expected, and is valid only for distances more than 20 nanometer (nm) away from the HJ. It is apparent that our analytic model produces the same DOS as the numerical method for the given potential. Clearly, the band offset substantially increases the DOS at locations within 20 nm from the HJ. For example, at 5 nm from the HJ and energies away from the band edge, the DOS obtained from our model is many orders of magnitude greater than the constant field result. Interestingly, as the distance from the HJ decreases, the DOS becomes independent of the field strength. As shown in Fig. 3, at 1 nm away from the HJ, the DOS (red solid curves) computed using the proposed model do not depend on the field strength, and are many orders of magnitude higher than those (black dash-dotted curves) computed using the constant field expression. Furthermore, the proposed DOS at 1 nm from the HJ coincides with the DOS (green dashed curves) of a step barrier with the same offset of 0.5 eV. This clearly demonstrates that, when very close to the HJ, the band offset determines the DOS, while the field strength has little effect.

The field enhancement factors, for potentials similar to the inset potential of Fig. 2, were computed as a function of electric fields at different locations using the proposed and Schenk models, as shown in Fig. 4. It is clear that, for locations 20 nm or more away from the HJ, the proposed and Schenk models produce nearly the same results. However, as the distance from the HJ decreases, the field enhancement factor computed using the proposed method increases dramatically, while the field dependence of the field factor decreases significantly. The location and field dependencies of the proposed field factor become more evident in Fig. 5. Clearly, the field factor increases nearly exponentially with decreasing distances for locations less than 20 nm away from the HJ. And it becomes independent of the field in the vicinity of the HJ. On the other hand, for locations more than 20 nm away from the HJ, the field factor does not depend on the location, but depends on the electric field.

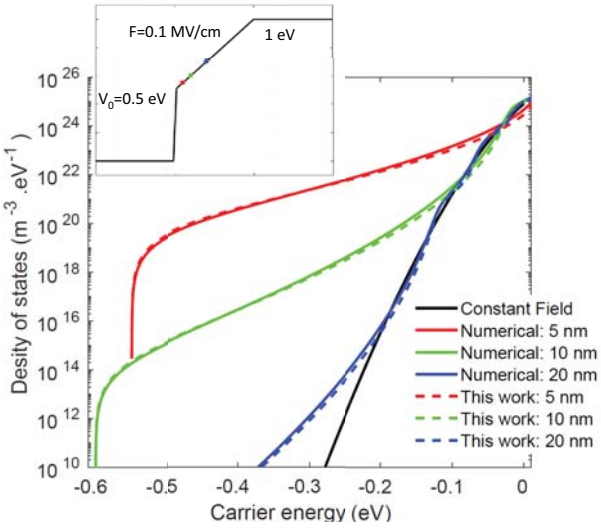

Fig. 2. 3D tunneling DOS for the inset potential at 5, 10, and 20 nanometer away from the HJ denoted by the colored dots. The zero energy is set to the barrier edge, and a more negative energy indicates further down from the barrier edge. The DOS were computed using the constant field expression [1] (black), the numerical code by Myers [7] that numerically solves the Schrodinger equation (color solid), and the analytic approach in this work (color dashed).

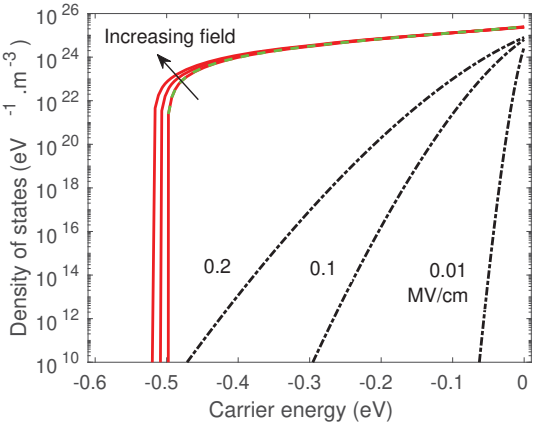

Fig. 3. 3D tunneling DOS for potentials similar to the inset potential in Fig. 2 at 1 nm away from the HJ with the field being 0.01, 0.1, and 0.2 MV/cm, respectively (red solid curves). The black dash-dotted curves correspond to the constant field DOS with the field value next to each curve. The green dashed curve corresponds to the DOS of a step barrier with $V_0 = 0.5$ eV.

To demonstrate the effect of the proposed band-to-trap tunneling model on device characteristics of HBTs, we simulated the Gummel current voltage curve of an $In_{0.5}Ga_{0.5}P$/GaAs NP^+N HBT utilizing *Charon*. The simulated device mimics the InGaP/GaAs HBT with the emitter-up configuration in [21]. The simulated collector and base currents are plotted in Fig. 6 as a function of base emitter voltages. We first used the standard SRH recombination in the emitter with a constant lifetime of 2×10^{-11} seconds for electrons and holes

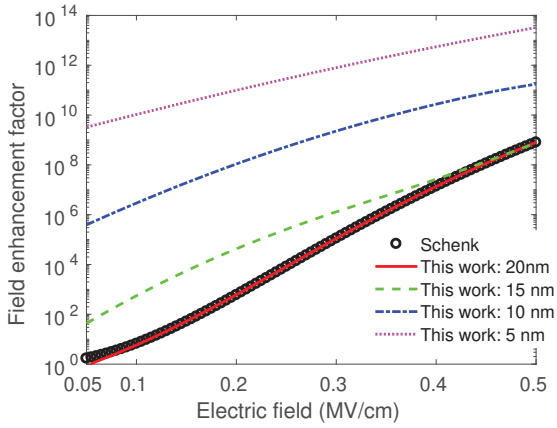

Fig. 4. Field enhancement factors as a function of electric fields for potentials similar to the inset potential of Fig. 2 at different locations. The red solid, green dashed, blue dash-dotted, and magenta dotted curves correspond to the 20, 15, 10, and 5 nm locations from the HJ, respectively, and were computed using the proposed model. Black dots are the results computed using the constant field Schenk model.

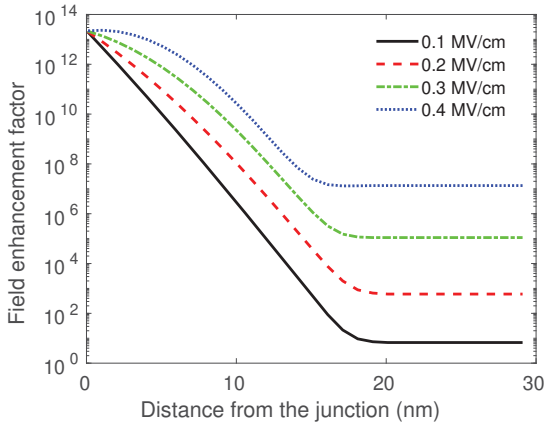

Fig. 5. Field enhancement factors computed using the proposed model as a function of the distances from the HJ for potentials similar to the inset potential of Fig. 2 at different electric fields.

to produce the base currents (red solid curve) that are similar to the experimentally observed base currents before neutron irradiation [7]. Next, we turned on the hole-to-trap tunneling in the emitter and assumed the traps were close to the mid-band gap of $In_{0.5}Ga_{0.5}P$, with the field independent $\tau(T, F = 0)$ set to 0.1 nanosecond for electrons and 1 nanosecond for holes. The resulting base currents obtained using the Schenk and proposed models are shown as the green dashed curve and the blue dash-dotted curve, respectively, in Fig. 6. Although the collector currents (black curve) do not change with the hole-to-trap tunneling near the emitter base junction, the base currents depend strongly on the hole-to-trap tunneling there. It is seen that, for the same simulation conditions, the proposed band-to-trap tunneling model predicts much larger base currents than the Schenk model. This is because the hole-to-trap tunneling from the base to the emitter is substantially enhanced by the

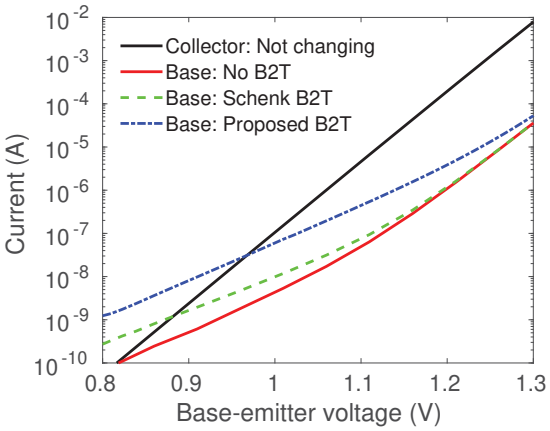

Fig. 6. Simulated collector and base currents as a function of base emitter voltages for an InGaP/GaAs NPN HBT with zero base collector bias.

emitter base junction band offset. We also see that the base currents predicted by the proposed model qualitatively agree with the experimentally measured base currents after neutron irradiation in [7].

IV. Conclusion

In summary, we have developed an analytic band-to-trap tunneling model that explicitly includes the effects of both electric field and band offset, based on the open boundary scattering approach. Our model is applicable to all one dimensional potentials, which can be approximated to a good degree such that the approximate potentials result in piecewise analytic wave functions with open boundary conditions. The model can be easily implemented into TCAD device and circuit simulators, thanks to its analytic form. It has been implemented into *Charon*, a MPI parallel TCAD code developed at Sandia National Laboratories. Using the model, we demonstrate that the band-to-trap tunneling strength (via the field enhancement factor) is dramatically increased at locations less than 20 nm away from a heterojunction (HJ), due to the band offset enhancement, when compared to the Schenk model. Furthermore, the field factor computed using the proposed model increases nearly exponentially with decreasing distances from the HJ, and becomes independent of the field when very close to the HJ. Simulation results of an InGaP/GaAs HBT using *Charon* show that the model predicts much larger base currents than the Schenk model. This is because the hole-to-trap tunneling is greatly enhanced by the emitter base junction band offset. The results are consistent with experimental observations.

Acknowledgment

We sincerely thank Samuel Myers, William Wampler, and Normand Modine for their insightful discussions regarding the physics. Special thanks go to Samuel Myers for providing the numerical code that was used for verifying our proposed density of states model. We would also like to thank Eric Keiter, Jason Gates, and Kara Peterson, for their helpful

discussion. This work is funded by the Advanced Scientific Computing (ASC) program at Sandia National Laboratories. Sandia National Laboratories is a multimission laboratory managed and operated by National Technology and Engineering Solutions of Sandia, LLC., a wholly owned subsidiary of Honeywell International, Inc., for the U.S. Department of Energy's National Nuclear Security Administration under contract DE-NA-0003525.

The views expressed in the article do not necessarily represent the views of the U.S. Department of Energy or the United States Government.

REFERENCES

[1] A. Schenk, "An improved approach to the Shockley-Read-Hall recombination in inhomogeneous fields of space-charge regions," J. Appl. Phys., vol. 71, pp. 3339–3349, April 1992.

[2] T. Yajima and L. Esaki, "Excess noise in narrow germanium p-n junctions," J. Phys. Soc. Jpn, vol. 13, pp. 1281–1287, 1958.

[3] J. R. Waterman, R. J. Wagner, and J. M. Perez, "Magnetic field effects on trap-assisted tunneling in $Hg_{0.78}Cd_{0.22}Te$ metal-insulator smiconductor capacitors," J. Vac. Sci. Technol. A, vol. 7, pp. 381–386, March 1989.

[4] A. Schenk, "A model for the field and temperature dependence of Shockley-Read-Hall lifetimes in silicon," Solid-State Electron., vol. 35, pp. 1585–1596, 1992.

[5] G. A. M. Hurkx, D. B. M. Klaassen, and M. P. G. Knuvers, "A new recombination model for device simulation including tunneling," IEEE Trans. Electron Devices, vol. 39, pp. 331–338, February 1992.

[6] E.g. Synopsys Sentaurus Device and Silvaco Atlas.

[7] S. M. Myers, W. R. Wampler, and N. A. Modine, "Recombination by band-to-defect tunneling near semiconductor heterojunctions: A theoretical model," J. Appl. Phys., vol. 120, art. 134502, 2016.

[8] M. Lundstrom, Fundamentals of Carrier Transport, 2nd ed., Cambridge: University Press, 2000, pp. 26.

[9] S. Datta, Electronic Transport in Mesoscopic Systems, 5th ed., Cambridge: University Press, 2003, pp. 155.

[10] B. Donner, M. Kleber, C. Bracher, and H. J. Kreuzer, "A simple method for simulating scanning tunneling images," AM. J. Phys., vol. 73, pp. 690–700, 2005.

[11] X. Gao, A. Huang, and B. Kerr, "Efficient band-to-trap tunneling model including heterojuntion band offset," ECS Trans., vol. 80, pp. 1005–1015, 2017.

[12] M. A. M. de Aguiar, "Exact Green's function for the step and square-barrier potentials," Phys. Rev. A, vol. 48, pp. 2567–2573, 1993.

[13] X. Gao, A. Huang, and B. Kerr, "Analytic band-to-trap tunneling model including band offset for heterojunction devices," unpublished.

[14] M. Abramowitz and I. A. Stegun, Handbook of Mathematical Functions, 10th ed., National Bureau of Standards, 1972, pp. 888, 25.4.33.

[15] W. Gander and W. Gautschi, "Adaptive quadrature - revisited," BIT Numeric. Math., vol. 40, pp. 84–101, March 2000.

[16] P. Bochev, K. Peterson, and X. Gao, "A new control volume finite element method for the stable and accurate solution of the drift-diffusion equations on general unstructured grids," Comput. Methods Appl. Mech. Engrg., vol. 254, pp. 126–145, 2013.

[17] A. N. Brooks and T. J. R. Hughes, "Streamline upwind/petrov-galerkin formulations for convection dominated flows with particular emphasis on the incompressible navier-stokes equations," Comput. Methods Appl. Mech. Engrg., vol. 32, pp. 199–259, 1982.

[18] P. Bochev and K. Peterson, "A parameter-free stabilized finite element method for scalar advection-diffusion problems," Cent. Eur. J. Math., vol. 11, pp. 1458–1477, 2013.

[19] X. Gao, D. Mamaluy, P. R. Mickel, and M. Marinella, "Three-dimensional fully-coupled electrical and thermal transport model of dynamic switching in oxide memristors," ECS Trans., vol. 69, pp. 183–193, 2015.

[20] X. Gao, D. Mamaluy, E. C. Cyr, and M. J. Marinella, "Comprehensive assessment of oxide memristors as post-CMOS memory and logic devices," ECS Trans., vol. 72, pp. 49-58, 2016.

[21] S. Choi, G. M. Peake, G. A. Keeler, K. M. Geib, R. D. Briggs, T. E. Beechem, R. A. Shaffer, J. Clevenger, G. A. Patrizi, J. F. Klem, A. Tauke-Pedretti, and C. D. Nordquist, "Thermal design and characterization of heterogeneously integrated InGaP/GaAs HBTs," IEEE Trans. Compon., Packag., Manuf. Technol., vol. 6, pp. 740–748, 2016.